RESEARCH   **Open Access**

Check for updates

Inflammatory damage caused by Echovirus 30 in the suckling mouse brain and HMC3 cells

Jichen Li[1,2], Yanjun Zong[1,2,3], Tiantian Sun[1,2,3], Ying Liu[1,2], Rui Wang[1,2], Jianfang Zhou[1], Qiang Sun[1,2*] and Yong Zhang[1,2*]

Abstract

Echovirus 30 (E30), a member of the species B *Enterovirus* family, is a primary pathogen responsible for aseptic meningitis and encephalitis. E30 is associated with severe nervous system diseases and is a primary cause of child illness, disability, and even mortality. However, the mechanisms underlying E30-induced brain injury remain poorly understood. In this study, we used a neonatal mouse model of E30 to investigate the possible mechanisms of brain injury. E30 infection triggered the activation of microglia in the mouse brain and efficiently replicated within HMC3 cells. Subsequent transcriptomic analysis revealed inflammatory activation of microglia in response to E30 infection. We also detected a significant upregulation of polo-like kinase 1 (PLK1) and found that its inhibition could limit E30 infection in a sucking mouse model. Collectively, E30 infection led to brain injury in a neonatal mouse model, which may be related to excessive inflammatory responses. Our findings highlight the intricate interplay between E30 infection and neurological damage, providing crucial insights that could guide the development of interventions and strategies to address the severe clinical manifestations associated with this pathogen.

Keywords Echovirus 30, HMC3 cells, Inflammatory response, PLK1

*Correspondence:
Qiang Sun
sunqiang8611@126.com
Yong Zhang
yongzhang75@sina.com
[1]National Key Laboratory of Intelligent Tracking and Forecasting for Infectious Diseases (NITFID), National Institute for Viral Disease Control and Prevention, Chinese Center for Disease Control and Prevention, Beijing 102206, China
[2]WHO WPRO Regional Polio Reference Laboratory, National Health Commission Key Laboratory for Biosafety, National Institute for Viral Disease Control and Prevention, Chinese Center for Disease Control and Prevention, 155 Changbai Road, Beijing 102206, China
[3]School of Basic Medical Sciences, Shandong Second Medical University, Weifang, China

Background

Enteroviruses (EVs), belonging to the order *Picornavirales* of the *Picornaviridae* family, are nonenveloped viruses with positive-sense single-stranded RNA genomes that include EV-A and EV-D [1]. Echovirus 30 (E30) is a common EV-B species that can cause various diseases, such as viral encephalitis, aseptic meningitis, hand, foot, and mouth disease, and acute flaccid paralysis [2, 3]. Although neurological infections are the most common complication leading to severe symptoms, no vaccines or effective drugs are available [4].

EVs, such as poliovirus and enterovirus A71, can invade the central nervous system (CNS) and cause severe meningitis, brainstem encephalitis, inflammatory infiltration, and gliosis [5–7]. Many cases of CNS infections caused by E30 outbreaks have been reported in Europe [8], and pathological evidence suggests that E30 can infect human choroid plexus epithelial cells

Li *et al. Virology Journal*   (2024) 21:165

Page 2 of 10

and disrupt the blood-brain barrier [9, 10]. E30 can cause paralysis and death in suckling mice. However, the exact mechanism underlying E30-induced neurological damage remains unclear [11]. Therefore, the mechanism by which host-cell interactions affect viral replication and pathogenesis must be further investigated [12].

Microglia, macrophage-like brain immune cells of the CNS, serve as viral reservoirs that promote excessive cellular stress and cytotoxicity [13]. When microglia encounter immunological stimuli, they activate and release inflammatory mediators such as Interleukin 6 (IL6). Increasing evidence indicates that the activation and subsequent dysregulation of these cells can lead to significant neurotoxic effects. In previous investigations of mouse brain tissue infected with EV-A71, co-localization of viral antigens with microglia was observed. Therefore, we speculate that the activation of microglia induced by E30 infection may be the mechanism driving the neuroinflammatory process [14, 15].

Despite increasing evidence, the specific mechanisms by which E30 infection damages the CNS remain unknown. In this study, we demonstrated that E30 infection directly infects human microglia and induces inflammatory responses. In addition, we identified PLK1 as a potential host factor affecting E30 replication, revealing a connection between E30 infection and neurological damage and providing crucial insights into clinical intervention strategies.

Materials and methods

Cell culture and virus

Human rhabdomyosarcoma (RD) and Human microglial clone 3 (HMC3) cell lines were commercially obtained from ATCC and cultured in Dulbecco's modified Eagle's medium (Gibco, USA) containing 10% fetal bovine serum (Gibco, USA) and 1% penicillin-streptomycin (HyClone, USA) at 37 °C in an atmosphere containing 5% CO_2.

The E30 strain TL1C/NM/CHN/2016 (TL1C) was isolated from an aseptic meningitis outbreak in Tongliao City, Inner Mongolia Autonomous Region, China, between June and August 2016.

Animal experiments

$IFNAR^{-/-}$ mice were purchased from SPF Biotechnology Co., Ltd. (Beijing, China). Three-day-old $IFNAR^{-/-}$ mice were intracranially (i.c.) infected with the E30 strain TL1C at 10^5 50% tissue culture infective dose ($TCID_{50}$) ($n=7$ per group). In contrast, control mice were inoculated with maintenance culture media and reared separately from the infected mice. The weights, survival rates, and clinical scores of mice were recorded daily. The clinical disease grade was scored as previously reported [16].

Intracranial injection of BI2536 or dimethyl sulfoxide (DMSO) was performed 4 h before E30 challenge. Comparative analyses of body weight, survival rates, and clinical scores were performed by injecting E30 or cell culture maintenance medium with DMSO. The groups included to five treatment groups: E30, E30+DMSO, E30+BI2536, BI2536, and DMSO, respectively.

Virus isolation and titers in mouse brain tissues

Brain tissues were harvested from 3-day-old $IFNAR^{-/-}$ mice intracranially injected with TL1C on days 1, 3, and 5 dpi ($n=7$ per time point). All samples were added to phosphate-buffered saline (PBS) containing 1% penicillin-streptomycin and crushed in a tissue grinder (Scientz, Ningbo, China). After three freeze-thaw cycles and subsequent centrifuging at 3000 g for 5 min at 4 °C, supernatants from each time point underwent 10-fold serial dilution and were inoculated into RD cells cultured in 96-well plates. After 5 days of observation, virus titers were evaluated using a $TCID_{50}$ assay.

Viral growth kinetics

HMC3 cells were infected with E30 (MOI=5) under 5% CO_2 and 37℃. After 2 h of incubation, cells were washed three times with PBS. Supernatants were collected 2, 12, 24, and 48 h post-infection (hpi) ($n=7$ per time point), and viral titers were quantified.

Histopathological and immunofluorescence assays

Following the i.c. injection of TL1C into 3-day-old $IFNAR^{-/-}$ mice, brain tissue from the experimental and control groups were harvested at 5 dpi. These tissues were fixed in formalin buffer for 24 h, dehydrated, embedded in paraffin, and sliced into 5 µm-thick sections. Hematoxylin and eosin (H&E) or Nissl's stains were applied to visualize the samples using an AxioCam MRc5 (Carl Zeiss, Berlin, Germany) at 200× or 400× magnification.

For immunofluorescence analysis, tissues were fixed in a 10% paraformaldehyde solution for 24 h, embedded in optimal cutting temperature (OCT) compound, and sectioned. OCT-embedded sections were stained with primary antibodies at 4 °C overnight. The primary antibodies were as follows: Rabbit polyclonal anti-E30 antibody (1:100 dilution) (ABclonal, Woburn, MA, USA), mouse monoclonal anti-GFAP antibody (1:100 dilution; Abcam, Cat No. ab4648, UK), and mouse monoclonal anti-Iba 1 antibody (1:100 dilution; GeneTex, Cat No. GTX10312, USA). Fluorescent DyLight 488, goat anti-rabbit IgG and Dylight 680, and

goat anti-mouse IgG (1:500 dilution) antibodies were added and incubated at 37 °C for 1 h. Finally, all images were collected using a Leica laser scanning confocal microscope (Leica, Germany).

Western blotting

Mouse brain tissue samples were homogenized in radio-immunoprecipitation assay (RIPA) buffer containing 1× protease inhibitor (Sigma, P8340). Tissue lysates were diluted in 1× SDS sample buffer and sonicated for 10 s after incubation at 100 °C for 10 min. Total lysate proteins were resolved in 4–20% Tris-glycine gels (Invitrogen) and transferred to nitrocellulose membranes. Western blotting was performed using an enhanced chemiluminescence (ECL) Prime kit (GE Healthcare). Multiple samples on the same membranes were probed with antibodies against the proteins of interest and β-actin, which served as the loading control. The primary monoclonal antibodies included mouse anti-Iba1 (GeneTex), anti-GFAP (Abcam), and anti-β-actin (Santa Cruz Biotechnology). while the secondary antibodies were obtained from Santa Cruz Biotechnology. The relative expression of target proteins to the internal controls was quantified using ImageJ software.

Cell toxicity analyses

After covering the 96-well plate with a single layer of cells, BI2536 (2, 5, 10, 20, 40, 80, 160, and 320 nM) was added after gradient dilution. After 48 h of incubation, 10 mL of CCK8 solution was added to the experimental, control, and blank wells. After another hour of incubation, each well's optical density (OD) was measured using a Multiskan FC enzyme-linked immunosorbent assay (Thermo Scientific). The cell activity at the corresponding inhibitory concentration was calculated based on the measured OD value to obtain the optimal inhibitory concentration.

Library preparation for transcriptome sequencing

TRIzol Reagent was used to extract total RNA from E30-infected HMC3 cells and the control group ($n=3$ per group). RNA concentrations were quantified using a Qubit 2.0 (Invitrogen, USA), and the RNA integrity (RIN≥8) was assessed using a Bioanalyzer 2100 (Agilent, USA). The initial cDNA strand was synthesized using random primer reverse transcription, followed by the amplification of second-strand cDNAs using RNase H and DNA polymerase. Finally, the enriched and purified cDNAs were sequenced on an Illumina NovaSeq 6000 platform. Gene expression levels were quantified using feature count software (version 1.5.0).

RNA-seq data analysis

Reads featuring perfect matches or single mismatches were considered for subsequent analysis and annotation against the *Homo sapiens* reference genome. The Hisat2-StringTie-Edge R pipeline facilitated read mapping, transcript assembly, and differential expression identification, respectively. Gene expression was normalized using fragments per kilobase of transcript per million. A significance threshold of $P<0.05$ and log2 (fold change)≥1.5, as analyzed using Hiplot Enhanced MA v0.1.0, was set as the threshold for significant differential expression. Gene Ontology (GO) and Kyoto Encyclopedia of Genes and Genomes (KEGG) pathway analyses were conducted to elucidate the biological significance of differentially expressed genes (DEGs). KEGG pathway analysis was used to better correlate the DEG catalog with system functions at higher levels of cells, species, and ecosystems to better understand the molecular response networks of protein-coding genes. These were then enriched and analyzed using the Database for Annotation, Visualization, and Integrated Discovery (DAVID) Bioinformatics Resources 6.8.

ELISA

Serum samples were collected from mice 1, 3, and 5 days after infection, and used to measure the expression of IL6, IFN-g, TNF-a and IL-1b by ELISA (Yeasen Biotechnology) according to the manufacturer's instructions. All experimental measurements were repeated seven times independently. Independent experiments were performed for each experiment.

RT-qPCR

Total RNA was extracted from HMC3 cells infected with the virus and reverse transcribed into cDNA. The reaction system was prepared using SYBR® Green ERTM qPCR Super Mix (Invitrogen) and detected using a fluorescence quantitative PCR instrument (reaction program: 50℃ 2 min, 95℃ 10 min; 95℃ 15s, 60℃ 1 min, 40 cycles). The expression levels of the detected genes were analyzed using the $2^{-\Delta\Delta Ct}$ method, with β-actin as the internal reference to compare the differential expression of the selected genes to that of the control group. All experimental measurements were repeated five times independently. Independent experiments were performed for each experiment.

Statistical analysis

GraphPad Prism 8.0 (GraphPad Software) was used for all statistical analyses. The log-rank (Mantel-Cox) test was used to assess survival rates among the various mouse groups. The statistical significance of the comparison of two means was assessed using the unpaired Student's t-test. The results were expressed as the

Table 1 Primers for RT-qPCR

Gene name	Primer	Primer sequence (5´-3´)
IL6	F	AGACAGCCACTCACCTCTTCAG
	R	TTCTGCCAGTGCCTCTTTGCTG
NLRP3	F	TGCACTGACTGGCAGAAGGC
	R	CCACATGCCGAGGATGGTCC
IL1A	F	GGCCCACTCCATGAAGGCTG
	R	GTCATTGGCGATGGCCTCCA
IFI16	F	AGCTGAGAGCCATCCCCACA
	R	CAGCTGGGCCTATGCTGGTC
CXCL8	F	GTGGCTCTCTTGGCAGCCTT
	R	CCACAACCCTCTGCACCCAG
CXCL1	F	TGCTGCTCCTGCTCCTGGTA
	R	GTCCGGGGGACTTCACGTTC
PLK1	F	AAGAGATCCCGGAGGTCCTA
	R	GCTGCGGTGAATGGATATTT

mean±standard deviation (SD). Independent experiments were performed for each experiment. Differences in cytokines and tissue viral titers in different mice in different mice were analyzed using the ANOVA test, with P values<0.05 deemed significant. $^{**}P<0.01$; $^{***}P<0.001$; $^{****}P<0.0001$; ns: No significant difference.

Results

E30 infection causes brain injury in a mouse model

We observed that the 3-day-old IFNAR$^{-/-}$ mice inoculated with a lethal dose of the E30 strain TL1C via the i.c. route developed significant hind limb paralysis, gradually lost weight, and died within 3–5 dpi with a clinical score of 3–5 (Fig. 1A). In contrast, the mock group remained healthy throughout the experiment (Fig. 1B, C).
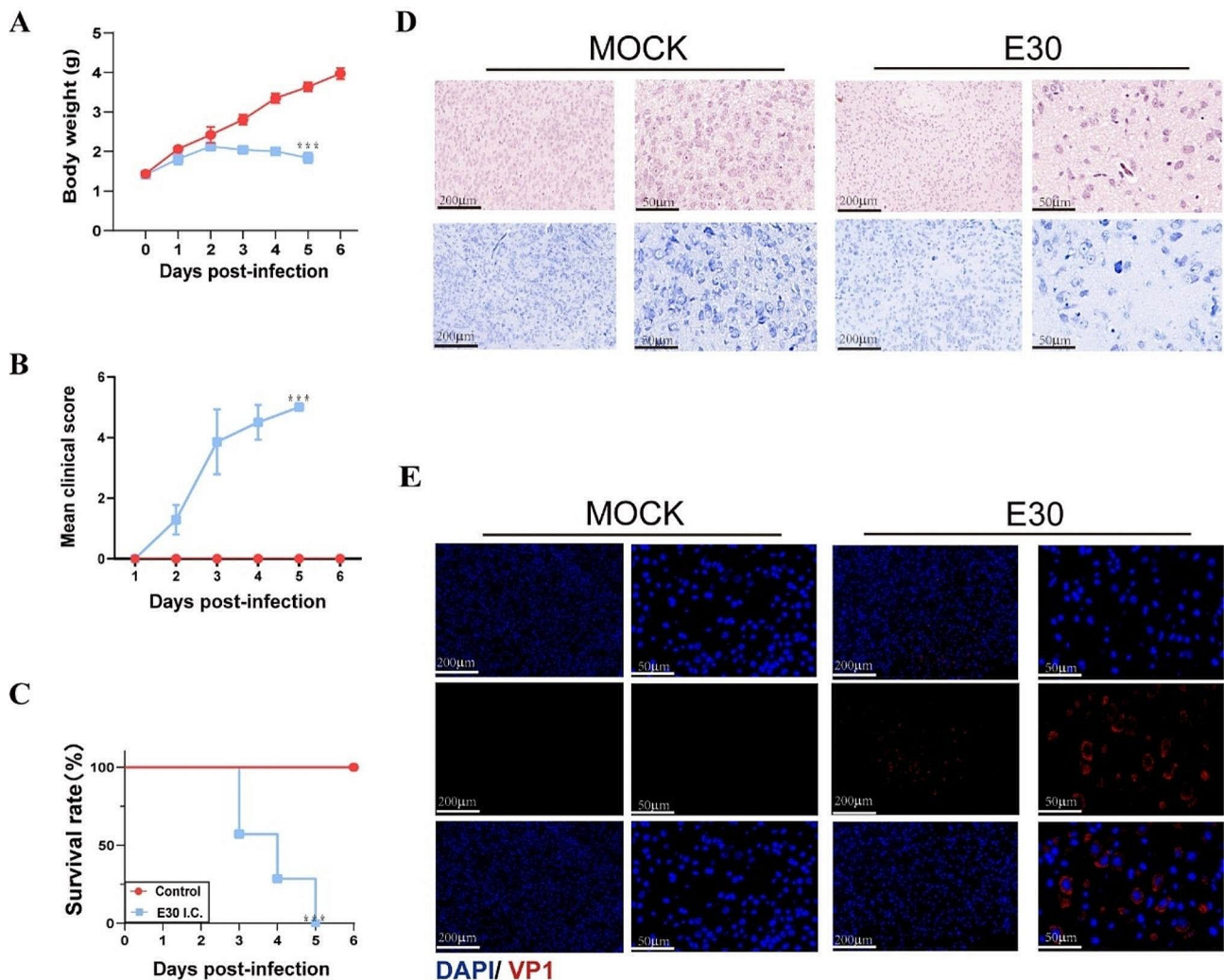

Fig. 1 E30 infection induces brain injury in a mouse model. Three-day-old IFNAR$^{-/-}$ mice were intracranially (i.c.) injected with TL1C strain at 10^5 TCID$_{50}$; ($n=7$ per group). Control mice received uninfected culture medium. The body weight (**A**), survival rate (**B**), and clinical scores (**C**) of the 3-day-old mice were monitored daily. Histopathological examination was performed on brain tissue from infected mice using H&E and Nissl's staining. Histopathological analysis revealed cerebral edema, neuronal cell swelling, diminished or absent Nissl bodies, and nuclear vacuolation (**D**). Mock tissues displayed no alterations. Brain tissue sections from suckling mice were immunofluorescence stained with DAPI (blue) and VP1 (E; red)—scale bars: 200 µm, 50 µm. Data are shown as the mean±SD. $^{**}P<0.01$; $^{***}P<0.001$; $^{****}P<0.0001$; ns: Not significant

Subsequently, these two types of infected mouse tissue at 5 dpi were subjected to H&E or Nissl staining to monitor histopathological changes. Compared with the control group, the symptoms of encephalitis presenting as cerebral edema and neuronal cell swelling in the infected mice were similar to those observed in humans (Fig. 1D). EV infection can cause neuroinflammation and microglia, the resident macrophages of the CNS, serve as viral reservoirs and promote excessive cellular stress and cytotoxicity [17]. Concordantly, the immunofluorescence analysis conducted in this study revealed that the E30 VP1 antigen colocalized with the mouse brain tissue (Fig. 1E). Our findings suggest that E30 infection can cause brain injury in neonatal mice.

Effective E30 replication and associated neurological pathological damage in infected mouse brains

Subsequently, we investigated whether E30 infection could cause gliosis and excessive inflammation in the spinal cord. We observed that the E30 VP1 antigen, compared to GFAP-positive astrocytes, colocalized with Iba1 positive microglia (Fig. 2A, B), and the viral loads in brain tissues ranged from $10^{1.5}$TCID$_{50}$ at 1 dpi to $10^{3.75}$TCID$_{50}$ at 5 dpi, suggesting effective replication of E30 in suckling mouse brains (Fig. 2C).

Likewise, we found that viral infections significantly activated the expression of IL6, IFN-g, TNF-a and IL-1b (Fig. 2D).

Compared to the control group, western blot analysis revealed increased expression of the GFAP and Iba1 proteins at 5 dpi (Fig. 2E). These results suggest that E30 infection causes excessive brain inflammation.

E30 replication and dysregulation of inflammatory signaling in HMC3 cells

Given the co-localization of the E30 VP1 antigen with Iba1-positive microglia in infected mouse brains, we next determined the replication potential of E30 in human microglial cell lines. We monitored the dynamics of viral replication in HMC3 cells, assessing viral titers at four-time points after infection. E30 exhibited replication in HMC3 cells, and the growth curve showed titers ranging from $10^{2.5}$ to $10^{5.5}$ TCID$_{50}$ (Fig. 3A).

With E30 exhibiting proficient replication in HMC3 cells, we further investigated how host-cell interactions influence viral replication and pathogenesis. Accordingly, we identified DEGs elicited by E30 infection in human HMC3 cells using RNA-seq analysis. In addition, 1284 genes were significantly upregulated and 831 genes were downregulated (Fig. 3B).

Through GO and KEGG pathway enrichment analyses of DEGs identified via RNA-seq of E30-infected HMC3 cells, we observed that signaling pathways associated with antiviral responses and inflammation were

significantly impacted (Fig. 3C, D). These pathways are involved in various aspects such as inflammatory response, protein phosphorylation, protein tyrosine kinase activity, viral response, innate immunity, cellular response to interferon-gamma, Toll-like receptor signaling, cytokine-cytokine receptor interaction, and the PI3K-Akt pathway. Notably, the expression of several genes, including *IL6*, interferon-gamma inducible protein 16 (*IFI16*), C-X-C motif chemokine ligand 8 (*CXCL8*), C-X-C motif chemokine ligand 1 (*CXCL1*), interleukin IL-1 alpha (*IL1A*), NLR family pyrin domain containing 3 (*NLRP3*), and polo-like kinase 1 (*PLK1*), exhibited substantial elevation following E30 infection (Table 1), which was confirmed by RT-qPCR (Fig. 3E). These genes contribute to the release of inflammatory factors during viral infection and also play pivotal roles in viral infection. Notably, the involvement of PLK1 in viral infection prompted us to explore its significance in E30 infection.

BI2536, a PLK1 inhibitor, alleviates pathogenic symptoms in E30-infected mice

Next, to determine the correlation between PLK1 and E30 replication, we investigated the effects of a PLK1 inhibitor (BI2536, a small-molecule PLK1 inhibitor) on the survival and viral replication of neonatal IFNAR$^{-/-}$ mice infected with a lethal dose of E30. The cell viability experiment and IC$_{50}$ indicated that the optimal inhibitor concentration that did not affect cell viability was 40 nM (Fig. 4D, E). Mice in the BI2536-treated group exhibited higher weights, higher survival rates, and lower clinical scores than those in the challenged group. Conversely, the values of the E30 and E30+DMSO groups did not exhibit significant differences (Fig. 4A, B, and C).

We conducted pathological examinations on brain tissue from all groups to gain deeper insights. Nissls and hematoxylin and eosin staining revealed no discernible pathological changes in the control group. Conversely, the E30-infected group showed substantially reduced nerve cell levels, accompanied by evident edema, bleeding, and vacuole-like changes. Notably, the BI2536-treated group exhibited less pronounced pathological alterations and virus titers than the challenged group (Fig. 4G, H, and F). These findings suggest a role for PLK1 expression in E30 replication, thereby offering a foundation for further exploration of the molecular pathogenic mechanisms of E30 during host infection.

Discussion

E30, a significant pathogen of aseptic meningitis, has received extensive attention across clinical medicine, epidemiology, and diagnostics [18, 19]. However, genotype variations appear to influence the prevalence and occurrence of viral meningitis outbreaks, contributing to the long-term neglect of E30 infection pathogenesis [20].
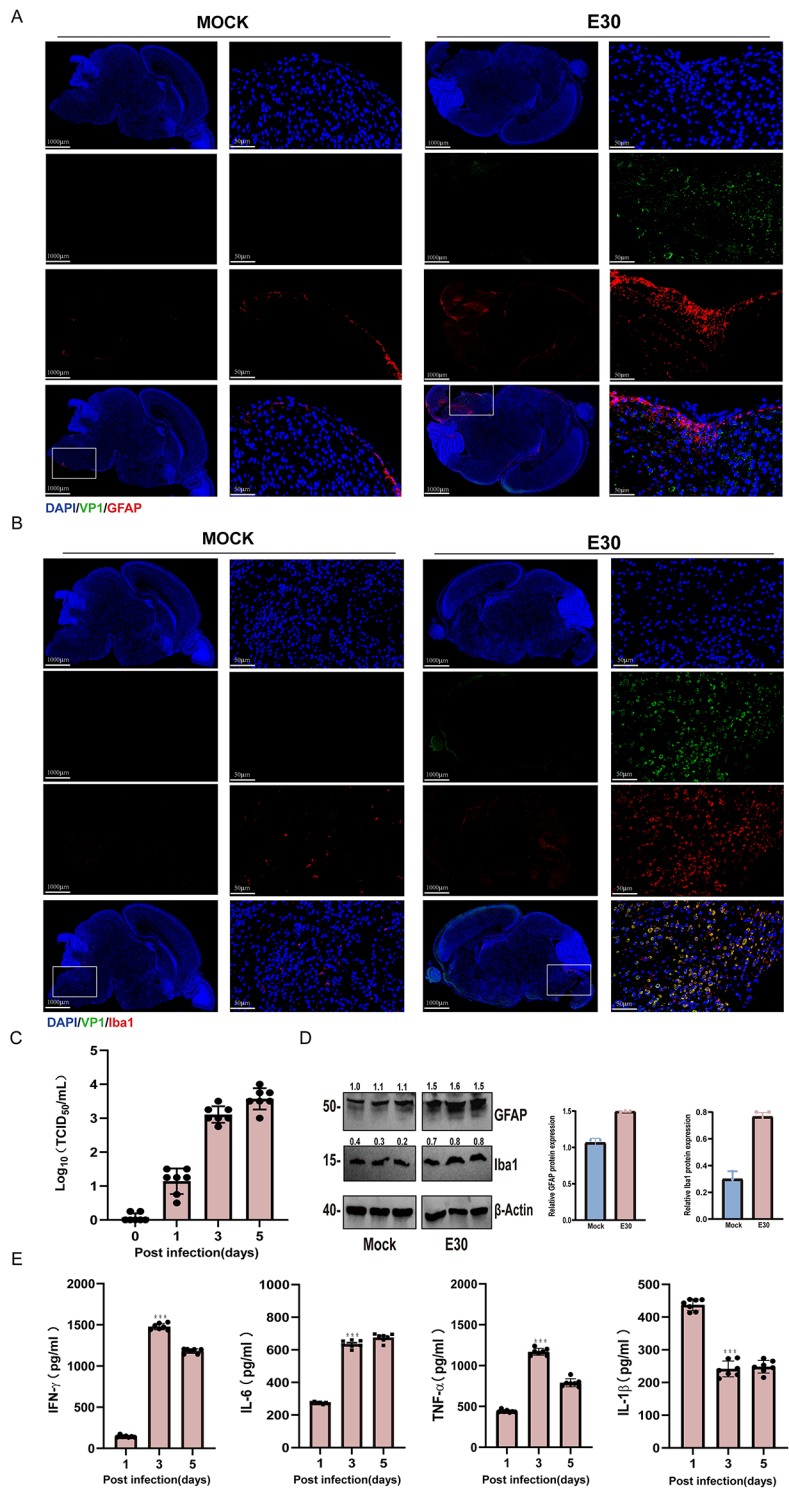
Fig. 2 Efficient E30 replication and associated neurological pathological damage in infected mouse brains. Three-day-old IFNAR$^{-/-}$ mice were i.c. injected with a 10^5 TCID$_{50}$ of E30. The spinal cords from suckling mice were immunofluorescence stained with DAPI (blue), astrocyte markers GFAP (**A**; red), microglia marker Iba1 (**B**; red), and VP1 (A, B; green). Scale bars: 1000 μm, 200 μm and 100 μm. Brain tissue virus titers were determined at 1, 3, and 5 days post-inoculation (dpi) (*n* = 7 at each time point), and ELISA was performed to determine the levels of IL6, IFN-g, TNF-a and IL-1b in mice (*n* = 7) (**C**, **E**). Western blot was applied to detect the expression of GFAP and Iba1 in mouse brains (**D**). The GFAP and Iba1 protein expression related to the internal control was quantified using Image J software. Data are shown as the mean ± SD. $^{**}P < 0.01$; $^{***}P < 0.001$; $^{****}P < 0.0001$; ns: Not significant
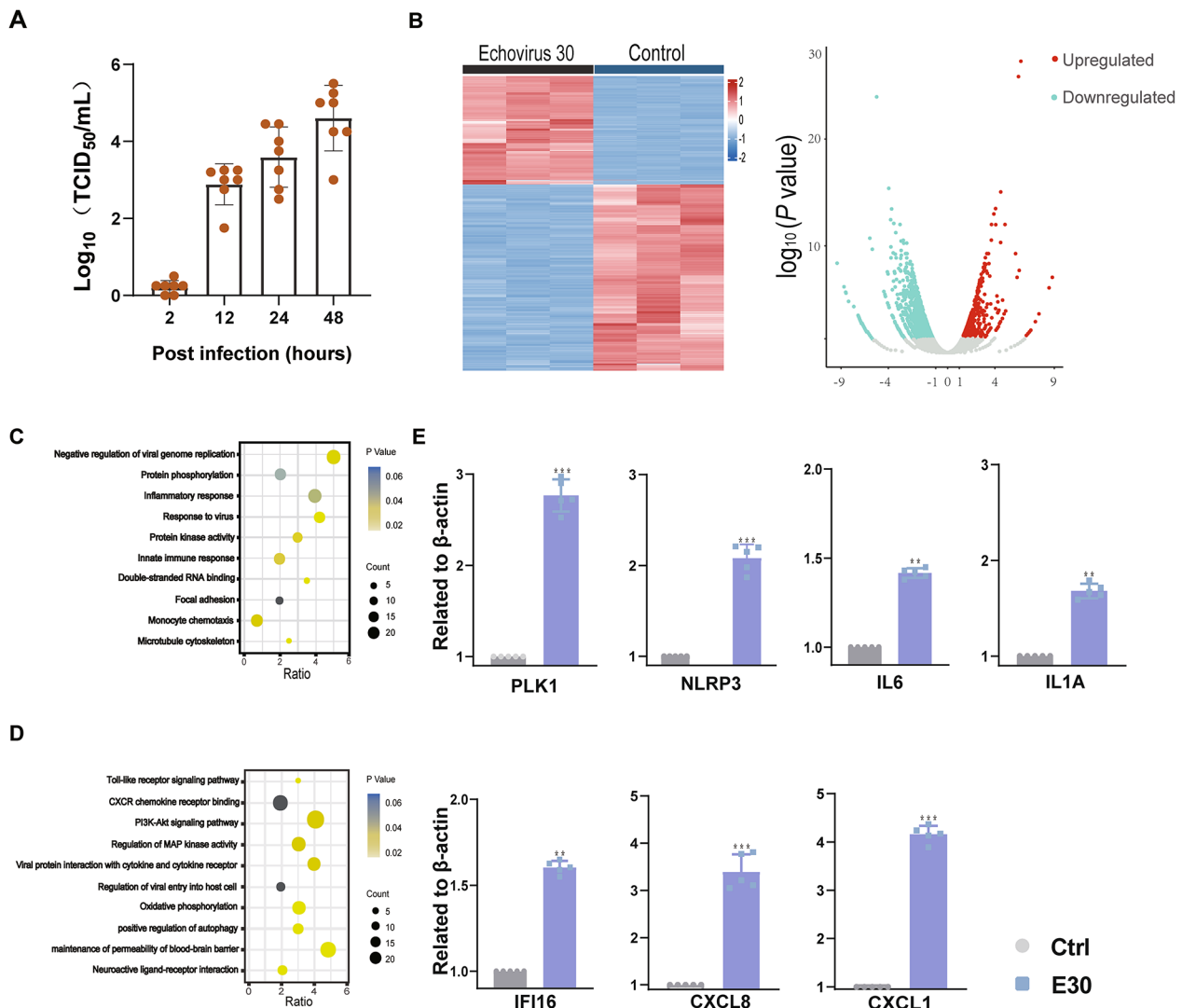
Fig. 3 Proficient replication of the E30 strain TL1C in HMC3 cells and dysregulation of inflammatory signaling and virus-responsive genes at the transcriptome level. Virus titer detection in E30-infected HMC3 cells ($n=7$ for each time point) (**A**). Volcano plot analysis for differentially expressed genes in E30-infected mice relative to the control group. Red dots denote up-regulated genes, whereas blue dots represent down-regulated genes (**B**). Gene Ontology (GO) enrichment and Kyoto Encyclopedia of Genes and Genomes (KEGG) pathway analyses of differentially expressed genes in HMC3 cells (**C**, **D**). RNA level by RT-qPCR ($n=5$) (**E**). Data are shown as the mean $\pm$ SD. $^{**}P < 0.01$; $^{***}P < 0.001$; $^{****}P < 0.0001$; ns: Not significant

Prior research has highlighted the potential of animal models to elucidate the possible mechanisms of EV infection, with EV-A71 and CVA16 mouse models serving as valuable tools for studying candidate vaccines and pathogenesis [21, 22]. EVs are usually not infectious to mice. Although various animal models of other EVs have been established, there are few models of Echovirus. Prior work by Bergelson et al. established an Echovirus type 1 mouse model [23], and our preliminary investigations have indicated significant pathological changes and mortality from E30 infection in suckling mice [11].

EVs, including E30, are linked to neurological diseases, thus posing a critical scientific challenge [3]. Virally induced inflammation within the CNS is believed to be mediated by autoreactive T cells activated in the peripheral region, infiltrating the blood-brain barrier [24, 25]. Infection with the TL1C strain of E30 is associated with symptoms such as lethargy, paralysis, and other CNS manifestations in IFNAR$^{-/-}$ mice, ultimately resulting in mortality. Although we previously established E30 replication within mouse brains, the precise mechanisms underlying the virus-mediated induction of CNS symptoms remain enigmatic and unknown [11]. Within the CNS, microglia and astrocytes are pivotal regulators of the neuroinflammatory process [26]. Notably, co-localization of the E30 VP1 antigen with Iba1-positive microglia was established, and further investigations confirmed the proficient replication of the TL1C isolate within
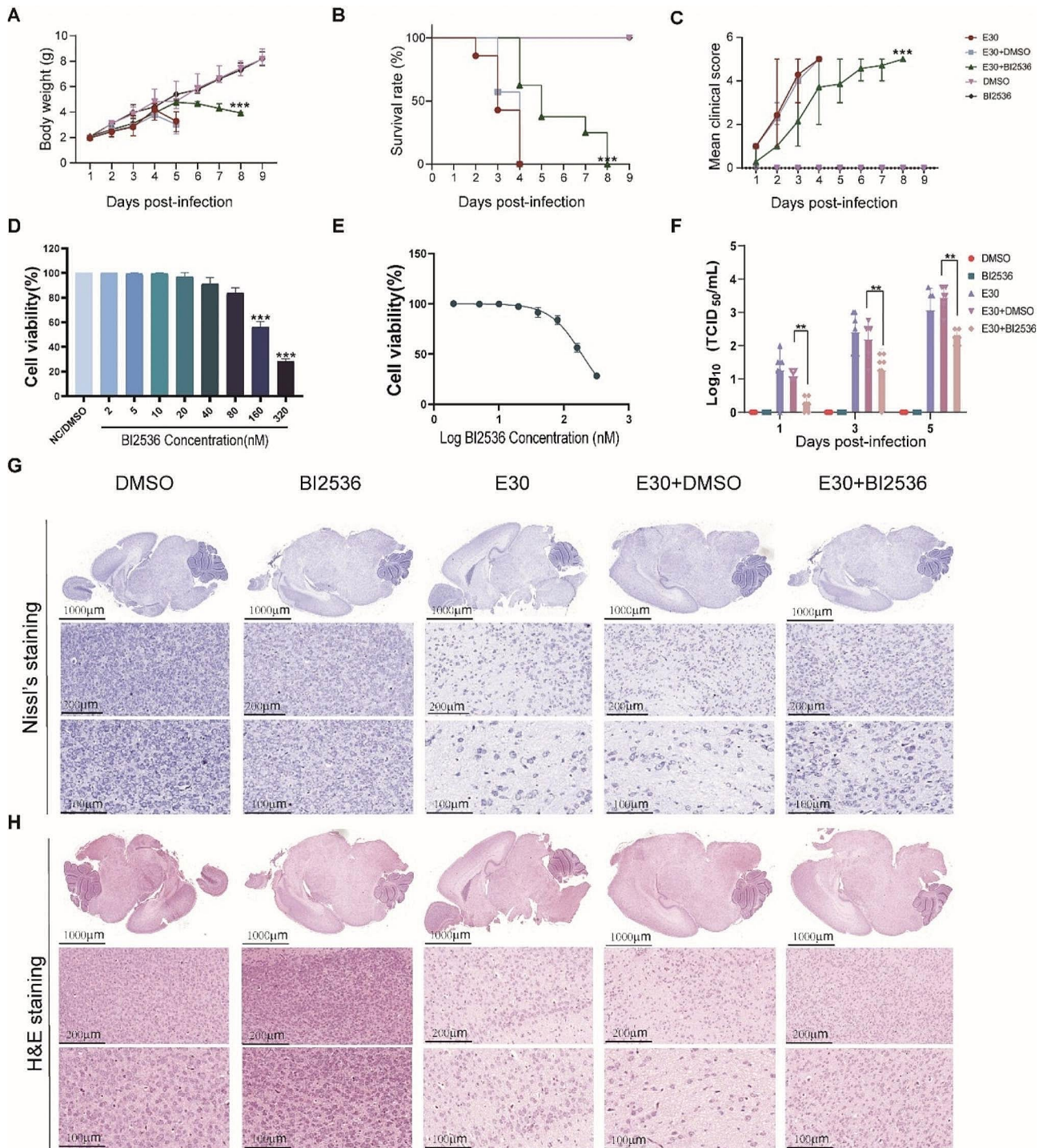
Fig. 4 PLK1 inhibitor BI2536 alleviates pathogenic symptoms in E30-infected mice. Monitoring of body weight (**A**), survival rates (**B**), and clinical scores (**C**) continued until 9 dpi. Cell viability and IC_{50} assays of BI2536 (**D**, **E**). Brain tissue virus titers were determined at 1, 3, and 5 days post-inoculation (dpi) with the BI2536 (*n* = 7 for each time point) (**F**). Nissl's and H&E staining of Spinal cord sections from E30-infected mice (**G**, **H**). Brain tissues collected from DMSO-treated, BI2536-treated, E30-infected, and DMSO + BI2536-treated E30 infection groups. E30-infected groups showed clear edema, bleeding, and vacuole-like changes (**H**). Scale bars: 1000 μm, 200 μm and 100 μm. Data represent the mean ± SD. Two-tailed Student's t-tests were employed to determine the significance of the data. $^{**}P < 0.01$; $^{***}P < 0.001$; $^{****}P < 0.0001$; ns: Not significant

Li *et al. Virology Journal*   (2024) 21:165

Page 9 of 10

HMC3 cells. As immune cells in the CNS, microglia play important roles in immune monitoring, debris clearance, and synaptic pruning in the central environment [27]. In addition, microglia exhibit significant morphological changes and interact with neurons and non-neurons in the CNS. The activation of microglia can lead to a series of neurological complications, and the dysfunction of microglia may adversely affect cognitive abilities, learning process, and memory retention. Therefore, the pro-inflammatory effect of microglia plays a pivotal role in elucidating the CNS symptoms caused by E30 infection [28, 29]. Subsequent RNA sequencing analysis of E30-infected HMC3 cells revealed dysregulation of inflammatory signaling and regulation of virus-related genes (IL6, IFI16, CXCL8, CXCL1, IL1A, NLRP3, and PLK1). IL6, IL1A, CXCL8, and CXCL1 are effective initiators of acute phase responses, and their rapid production helps enhance host defenses against infections and tissue damage. Excessive synthesis is associated with disease pathology [30, 31]. In the immune response activated by exogenous viral infection, IFI16 affects the activation of NLRP3 by triggering the STING pathway, which is related to the development of various inflammatory and immune-mediated diseases [32]. Notably, PLK1, a member of the polo-like kinase family, has been implicated in both the cell cycle and viral infection, thereby prompting further exploration into its pivotal role in E30 infection.

In addition to DEGs, PLK1 has been identified as a crucial player in multiple facets of mitosis, particularly in regulating mitotic entry and exit [33]. Moreover, it exerts regulatory control over interferon (IFN) induction via mitochondrial antiviral-signaling protein (MAVS). Given its significance in cell mitosis, the potential involvement of PLK1 in facilitating the cellular entry of E30 during infection is evident. This kinase governs mitotic entry, Spindle Assembly Checkpoint (SAC) silencing, and cytokine division [34, 35]. Research-based on anti-PLK1 antibodies and small interfering RNA (siRNA) treatments has highlighted the importance of PLK1 in the progression of cancer [36]. BI2536 can effectively bind to the kinase domain of PLK1 and inhibit its activity, including regulation of various mitotic processes and the cell cycle [37]. Although the mechanisms by which BI2536 inhibits E30 replication remain unclear, preliminary results suggest its potential to mitigate E30-induced pathological manifestations.

Conclusion
Our research explored the neuronal damage in the brains of suckling mice caused by E30 infection and the upregulation of inflammatory response pathways in HMC3 cells. Furthermore, we discovered that PLK1 may be necessary for viral infection. These findings offer further avenues for exploring the mechanisms by which E30 infection triggers CNS diseases. At present, the factors involved in E30 infection are not known and require further exploration.

Abbreviations
BBB	Blood-brain barrier
DAPI	4′,6-diamidino-2-phenylindole
DEG	Differentially expressed genes
DMSO	Dimethyl sulfoxide
ECL	Enhanced chemiluminescence
GFAP	Glial fibrillary acidic protein
GO	Gene Ontology
H&E	Hematoxylin and eosin
IFN	Interferon
IgG	Immunoglobulin G
KEGG	Kyoto Encyclopedia of Genes and Genomes
MOI	Multiplicity of infection
OCT	Optimal cutting temperature
PBS	Phosphate-buffered saline
PMA	Phorbol 12-myristate 13-acetate
RD	Rhabdomyosarcoma
$TCID_{50}$	50% tissue culture infective dose

Supplementary Information
The online version contains supplementary material available at https://doi.org/10.1186/s12985-024-02437-4.

Supplementary Material 1

Supplementary Material 2

Supplementary Material 3

Author contributions
Jichen L and Qiang S designed the study, performed the experiments, and prepared the manuscript. Zong Y, Liu Y, Sun T, and Wang R performed the experiments. Zhang Y and Sun Q designed the study and revised the manuscript. All the authors have read and approved the final manuscript.

Data availability
No datasets were generated or analysed during the current study.

Declarations

Ethics approval and consent for publication
All animal experiments were performed following the Chinese regulations for laboratory animals. Experimental protocols were approved by the Second Ethics Review Committee of the National Institute for Viral Disease Prevention and Control, Chinese Center for Disease Control and Prevention (Approval no. 20221012098).

Competing interests
The authors declare no competing interests.

References
1. Lefkowitz EJ, Dempsey DM, Hendrickson RC, Orton RJ, Siddell SG, Smith DB. Virus taxonomy: the database of the International Committee on Taxonomy of Viruses (ICTV). Nucleic Acids Res. 2018;46:D708–17.

Li *et al. Virology Journal*   (2024) 21:165

Page 10 of 10

2. Benschop KSM, Broberg EK, Hodcroft E, Schmitz D, Albert J, Baicus A, Bailly JL, Baldvinsdottir G, Berginc N, Blomqvist S, et al. Molecular Epidemiology and Evolutionary Trajectory of emerging Echovirus 30, Europe. Emerg Infect Dis. 2021;27:1616–26.

3. Chen J, Han Z, Wu H, Xu W, Yu D, Zhang Y. A large-scale outbreak of Echovirus 30 in Gansu Province of China in 2015 and its phylodynamic characterization. Front Microbiol. 2020;11:1137.

4. Vandesande H, Laajala M, Kantoluoto T, Ruokolainen V, Lindberg AM, Marjomaki V. Early entry events in Echovirus 30 infection. J Virol 2020, 94.

5. Jin Y, Li D, Sun T, Du Y, Gao Y, Ding R, Ji W, Zhang W, Yang H, Chen S, Duan G. Pathological features of Enterovirus 71-Associated brain and lung damage in mice based on quantitative proteomic analysis. Front Microbiol. 2021;12:663019.

6. Chen BS, Lee HC, Lee KM, Gong YN, Shih SR. Enterovirus and Encephalitis. Front Microbiol. 2020;11:261.

7. Uprety P, Graf EH. Enterovirus infection and acute flaccid myelitis. Curr Opin Virol. 2020;40:55–60.

8. Savolainen C, Hovi T, Mulders MN. Molecular epidemiology of Echovirus 30 in Europe: succession of dominant sublineages within a single major genotype. Arch Virol. 2001;146:521–37.

9. Rhoades RE, Tabor-Godwin JM, Tsueng G, Feuer R. Enterovirus infections of the central nervous system. Virology. 2011;411:288–305.

10. Rudolph H, Schroten H, Tenenbaum T. Enterovirus infections of the Central Nervous System in Children: an update. Pediatr Infect Dis J. 2016;35:567–9.

11. Li J, Zhang G, Sun Q, Zhang K, Lu H, Xiao J, Han Z, Zhao H, Xu W, Zhang Y, Liu Z. Pathological characteristics of Echovirus 30 infection in a mouse model. J Virol. 2022;96:e0012922.

12. Majer A, McGreevy A, Booth TF. Molecular pathogenicity of enteroviruses causing neurological disease. Front Microbiol. 2020;11:540.

13. McMillan RE, Wang E, Carlin AF, Coufal NG. Human microglial models to study host-virus interactions. Exp Neurol. 2023;363:114375.

14. Galland F, Seady M, Taday J, Smaili SS, Goncalves CA, Leite MC. Astrocyte culture models: Molecular and function characterization of primary culture, immortalized astrocytes and C6 glioma cells. Neurochem Int. 2019;131:104538.

15. Jin Y, Sun T, Zhou G, Li D, Chen S, Zhang W, Li X, Zhang R, Yang H, Duan G. Pathogenesis Study of Enterovirus 71 Using a Novel Human SCARB2 Knock-In Mouse Model. *mSphere* 2021, 6.

16. VanBlargan LA, Himansu S, Foreman BM, Ebel GD, Pierson TC, Diamond MS. An mRNA vaccine protects mice against multiple Tick-transmitted Flavivirus infections. Cell Rep. 2018;25:3382–e33923383.

17. Aguglia G, Coyne CB, Dermody TS, Williams JV, Freeman MC. Contemporary enterovirus-D68 isolates infect human spinal cord organoids. mBio. 2023;14:e0105823.

18. Broberg EK, Simone B, Jansa J. The Eu/Eea Member State C: Upsurge in Echovirus 30 detections in five EU/EEA countries, April to September, 2018. Euro Surveill 2018, 23.

19. Cosic G, Duric P, Milosevic V, Dekic J, Canak G, Turkulov V. Ongoing outbreak of aseptic meningitis associated with echovirus type 30 in the City of Novi sad, Autonomous Province of Vojvodina, Serbia, June - July 2010. Euro Surveill 2010, 15.

20. Mantadakis E, Pogka V, Voulgari-Kokota A, Tsouvala E, Emmanouil M, Kremastinou J, Chatzimichael A, Mentis A. Echovirus 30 outbreak associated with a high meningitis attack rate in Thrace, Greece. Pediatr Infect Dis J. 2013;32:914–6.

21. Xu Y, Ma S, Zhu L, Huang Z, Chen L, Xu Y, Yin H, Peng T, Wang Y. Clinically isolated enterovirus A71 subgenogroup C4 strain with lethal pathogenicity

22. Hooi YT, Ong KC, Tan SH, Perera D, Wong KT. Coxsackievirus A16 in a 1-Day-old mouse model of central nervous system infection shows lower neuro-virulence than Enterovirus A71. J Comp Pathol. 2020;176:19–32.

23. Bergelson JM, Shepley MP, Chan BM, Hemler ME, Finberg RW. Identification of the integrin VLA-2 as a receptor for echovirus 1. Science. 1992;255:1718–20.

24. Alexander JJ. Blood-brain barrier (BBB) and the complement landscape. Mol Immunol. 2018;102:26–31.

25. Dahm T, Adams O, Boettcher S, Diedrich S, Morozov V, Hansman G, Fallier-Becker P, Schadler S, Burkhardt CJ, Weiss C, et al. Strain-dependent effects of clinical Echovirus 30 outbreak isolates at the blood-CSF barrier. J Neuroinflammation. 2018;15:50.

26. Liddelow SA, Guttenplan KA, Clarke LE, Bennett FC, Bohlen CJ, Schirmer L, Bennett ML, Munch AE, Chung WS, Peterson TC, et al. Neurotoxic reactive astrocytes are induced by activated microglia. Nature. 2017;541:481–7.

27. Lukens JR, Eyo UB. Microglia and Neurodevelopmental disorders. Annu Rev Neurosci. 2022;45:425–45.

28. Tremblay ME. A diversity of cell types, subtypes and phenotypes in the Central Nervous System: the importance of studying their Complex relationships. Front Cell Neurosci. 2020;14:628347.

29. Tay TL, Bechade C, D'Andrea I, St-Pierre MK, Henry MS, Roumier A, Tremblay ME. Microglia gone Rogue: impacts on Psychiatric disorders across the Lifespan. Front Mol Neurosci. 2017;10:421.

30. Kang S, Tanaka T, Narazaki M, Kishimoto T. Targeting Interleukin-6 signaling in Clinic. Immunity. 2019;50:1007–23.

31. de Siqueira Santos R, Rochael NC, Mattos TRF, Fallett ESMF, Linhares-Lacerda L, de Oliveira LT, Cunha MS, Mohana-Borges R, Gomes TA, Barbosa-Silva MC, et al. Peripheral nervous system is injured by neutrophil extracellular traps (NETs) elicited by nonstructural (NS) protein-1 from Zika virus. FASEB J. 2023;37:e23126.

32. Bao H, Yan J, Huang J, Deng W, Zhang C, Liu C, Huang A, Zhang Q, Xiong Y, Wang Q, et al. Activation of endogenous retrovirus triggers microglial immuno-inflammation and contributes to negative emotional behaviors in mice with chronic stress. J Neuroinflammation. 2023;20:37.

33. Reid RJ, Du X, Sunjevaric I, Rayannavar V, Dittmar J, Bryant E, Maurer M, Rothstein R. A synthetic dosage Lethal Genetic Interaction between CKS1B and PLK1 is conserved in yeast and Human Cancer cells. Genetics. 2016;204:807–19.

34. Nilsson MB, Sun H, Robichaux J, Pfeifer M, McDermott U, Travers J, Diao L, Xi Y, Tong P, Shen L et al. A YAP/FOXM1 axis mediates EMT-associated EGFR inhibitor resistance and increased expression of spindle assembly checkpoint components. Sci Transl Med 2020, 12.

35. Petronczki M, Lenart P, Peters JM. Polo on the rise-from Mitotic Entry to Cytokinesis with Plk1. Dev Cell. 2008;14:646–59.

36. Shi W, Zhang G, Ma Z, Li L, Liu M, Qin L, Yu Z, Zhao L, Liu Y, Zhang X, et al. Hyperactivation of HER2-SHCBP1-PLK1 axis promotes tumor cell mitosis and impairs trastuzumab sensitivity to gastric cancer. Nat Commun. 2021;12:2812.

37. Wu M, Wang Y, Yang D, Gong Y, Rao F, Liu R, Danna Y, Li J, Fan J, Chen J, et al. A PLK1 kinase inhibitor enhances the chemosensitivity of cisplatin by inducing pyroptosis in oesophageal squamous cell carcinoma. EBioMedicine. 2019;41:244–55.

Publisher's Note